RSC Advances

ROYAL SOCIETY OF CHEMISTRY

www.rsc.org/advances

TOC

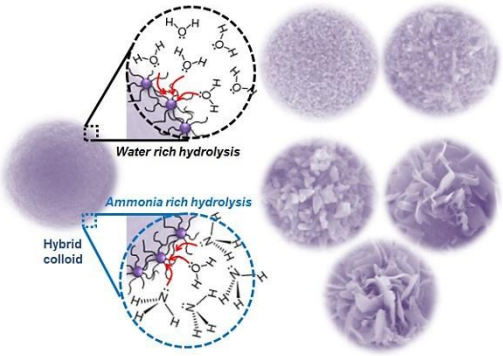

Tailoring solvent composition and concentration in solvothermal treatment enables effective control of morphological evolution of hierarchical titanium-oxide hybrid materials.

Journal Name

RSCPublishing

ARTICLE

An Effective Template-Free Synthesis Strategy for Hierarchical Titanium Oxide Hybrids: Tailoring Solvent Environment

Cite this: DOI: 10.1039/xoxxoooooox

Received ooth January 2012,
Accepted ooth January 2012

DOI: 10.1039/xoxxoooooox

www.rsc.org/

Sharon Y. Wang[a,†], Myo Tint Soe[a,†], Kevin T. Guo[a], Xiao Li Zhang[a,b,c]*, Zheng Xiao Guo[b,c]

Strategic tailoring of solvent mixtures in solvothermal synthesis harnessed hydrolysis kinetics and direction of crystal growth, leading to sophisticated morphological control of size, shape, porosity and overall texture of the resulting materials. The approach enabled successful preparation of hierarchical hybrid titanium oxides of diverse morphologies via a relatively simple low-cost template-free synthesis. Such synthesised materials exhibit superior specific surface areas of 106.2 – 639.4 m^2/g along with varied morphologies, in contrast to that of commercial Degussa P25 TiO_2 (ca. 60 m^2/g), and demonstrated promising efficiency and effectiveness in environmental applications, e.g. inorganic and organic pollutant removal from water and as a host for co-catalyst/photocatalyst.

Introduction

Over the past decades, hierarchically structured materials with well-defined nanoscale texture have shown increasing importance for an extensive range of practical applications, particularly in energy and environmental sustainability. This has catalysed extensive interest and rapid development of the design, fabrication and functionalization of a variety of hierarchical materials across worldwide scientific and commercial communities[1]. Among those, hierarchical titanium oxide based compounds/hybrids have significantly contributed to the recent development of highly efficient energy conversion systems, including catalysis/photocatalysis[2], organic and inorganic pollutants removal[3], solar cells[4], solar fuel generation[5], electrochemical or photoelectrochemical devices[6], lithium-ion batteries[7], supercapacitors[8], sensors[9], and so on[10]. This can be mainly attributed to its unique combination of superior surface structural features, excellent solution/gas accessibility, proven optical and electronic properties, along with reliable durability for real-life applications.

To date, fabrication techniques for hierarchical architectures still largely rely on template-directed methodologies utilizing either soft directing agents, such as block copolymers and micelles, or highly porous hard templates using carbon, aluminium oxide and SiO_2[11]. Although generally offering a reproducible structure, those techniques also require extra hazardous chemical/solvent, energy and processing steps to remove the fugitive template. Such procedures, as well as any template residuals, could unduly affect the quality of the final product.

In contrast, template-free synthesis approaches avoid the aforementioned drawbacks and offer a relatively simple, efficient and cost-effective way of making porous materials, which is highly desirable for both scientific research and industrial applications[12]. Here, we report a template-free synthesis strategy to generate hierarchical titanium oxide based materials. A wide range of morphologies were achieved through simply tailoring of the reaction solvent environment – including mesoscopic and microscopic textures with spiny, tubular and layered structures. The facile solution-phase reaction process enabled effective control of particle size, surface area, porosity, morphology and crystallinity of the hierarchical structures. The as-produced materials show far greater a specific surface area than the commercial P25 TiO_2 nanoparticles, leading to effective inorganic/organic pollutant removal and the formation of finely dispersed co-catalyst /-photocatalyst over the surfaces. The approach and the material demonstrate great potential for many environmental related applications.

Results and Discussion

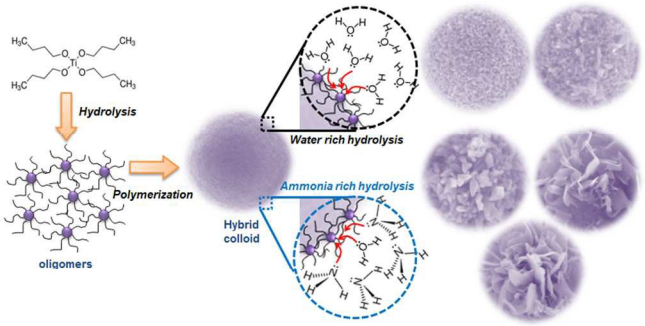

Scheme 1. Schematic of the formation mechanism of hybrid colloids (hybrid precursor spheres) and the subsequent phase transformations into hierarchical hybrid titanium oxide spheres.

Spherical hybrid precursors were synthesized through a sol-gel process which has been well documented in our previous report[13]. Detailed experimental procedures were shown in the Supplementary Information section. In a template-directed process, cooperative assemblies are responsible to the initial aggregation, which involve the interactions between the template directing agents and inorganic oligomers as well as the self-assembly of the hydrophobic alkyl chains of the agent molecules[14]. In contrast, in this work, the tetrabutyl orthotitanate moleculars $Ti(O(CH_2)_3CH_3)_4$ was carefully chosen to form relatively bulky $Ti(O(CH_2)_3CH_3)_{4-x}(OH)_x$ species and their oligomers through hydrolysis. These species/oligomers tend to aggregate to reduce the overall interface free energy. Minimization of surface free energy drives further polymerization of the titanium species/oligomers to form spherical colloids – the sub-micron sized hybrid precursors[15]. The SEM image in Figure 1 a) shows clearly the spherical morphology and relatively smooth surface of the hybrid precursors. As illustrated in Scheme 1, simply tailoring the solvent mixture for the solvothermal treatment of the hybrid precursor spheres enabled successful manipulation of a diverse range of morphology, pore size and porosity of the final hierarchically structured materials, as further elaborated in the following.

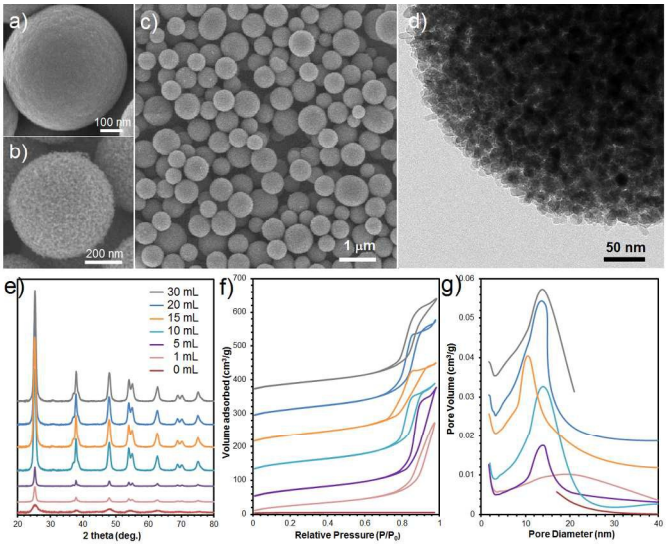

Fig 1. a) SEM image of the as-prepared precursor spheres; characteristics of spherical TiO_2 nanoparticle aggregates prepared by solvothermal treatment: b), c) and d) SEM and TEM images of sample treated in an ethanol:water solvent (1:1 volume ratio), **Sample T-H15**; and e) XRD patterns, f) nitrogen sorption isotherms and g) the corresponding pore size distribution of the mesoporous TiO_2 nanoparticle aggregates prepared by solvothermal treatment with varying water content in a total solution of 30 mL.

When the solvothermal treatment was conducted in an ethanol and water solvent mixture, the aggregated titanium oligomers were gradually hydrolysed, leading to a crystalline structure with well-developed surface roughness over the spheres, Figure 1 b). A low-magnification SEM image in Figure 1 c) shows that the hydrolysed spherical aggregates prepared from an ethanol:water solvent of a 1:1 volume ratio (denoted as **Sample T-H15**) are of around 400 – 800 nm in diameter, inherited from the precursor spheres. Within each spherical aggregate are particles of approximately 10-15 nm, forming a "worm-hole"-like network, as seen in Figure 1 d) under a mid-range TEM magnification.

Firstly, the amount of water in the solvent mixture largely influences the crystalline structure of the aggregates. Such solvent influence was analysed by microscopic morphology observations, XRD crystallography, and BET surface area, pore diameter and porosity characterisations. In Figure 1 e), the XRD patterns of the hydrolysed aggregates can be indexed to anatase TiO_2 (JCPDS card number 21-1272). The **Sample T-H0** from a pure ethanol solvent shows a type IV isotherm with a small hysteresis at low P/P_o in nitrogen gas sorption, indicating the nonordered interparticle mesoporosity of this sample. The hysteresis at low P/P_o corresponds to small mesopores of approximately 3.7 nm in the framework of the sample. The large surface area of over 300 m^2/g and a large pore volume of 0.23 cm^3/g confirmed this finding. The broad XRD humps with considerably low diffraction intensity in Figure 1 e) suggest poor crystallinity. This is also confirmed by TEM observations in Figures S1 a) and b), where no crystalline features or contrast can be identified.

When a small amount of water (< 2 mL, in a 30 mL solution) was used in the solvent mixture, the considerably higher solvent vapour generated from the excess ethanol is likely to promote agglomeration during the hydrolysis of the oligomers, leading to relatively large clusters. Since the very limited amount of water may not be sufficient for a crystalline refinement through diffusion and/or reorientation, such solvothermal treatment would end with a large particle size but poor crystalline structure. As shown in Figures S1 c) – f), much rougher surface features with individual particle size reaching approximately 50 nm were observed from the **Sample T-H1** and **Sample T-H2** of spherical aggregates, prepared using 1 and 2 mL water, respectively. While the relatively low peak intensity of the corresponding XRD patterns suggest the poor crystalline nature of the sample. Larger particles led to wider particle interspaces within the aggregates that were confirmed by estimated pore size distributions from BET analyses with major pore diameters of 14.9 and 17.1 nm corresponding to the use of 1 and 2 mL water in the solvent mixture, respectively.

Table 1. Physical properties of the spherical titanium oxide aggregates prepared with solvothermal treatment in the presence of varying water concentration.[a]

Sample	Water (mL)	S_{BET} (m^2/g)	PD (nm)	V_{sp} (cm^3/g)
T-H0	0	328.9	3.7	0.23
T-H1	1.0	111.8	14.9	0.51
T-H2	2.0	129.0	17.1	0.71
T-H5	5.0	119.0	14.7	0.56
T-H10	10.0	124.8	12.2	0.48
T-H15	15.0	132.4	9.4	0.38
T-H20	20.0	126.9	10.9	0.46
T-H25	25.0	113.2	11.6	0.42
T-H30	30.0	112.8	11.2	0.43

[a] S_{BET} = BET specific surface area obtained from N_2 adsorption data in the P/P_o range from 0.0666 to 0.2664. PD = average pore size determined using the BJH model from the N_2 adsorption data. V_{sp} = single-point pore volume calculated from the adsorption isotherm at P/P_o = 0.98.

With increasing water concentration in the solvent mixture, up to (50%, volume ratio of 1:1), crystalline structures were progressively developed along with a minor drop in the main pore size from around 14.7 to 9.4 nm, as indicated by the XRD analytical results (Figure 1e). Meanwhile all samples display a type IV isotherm and a H1 type hysteresis loop, indicating mesoporous characteristics of the aggregates. Surface areas of all TiO_2 nanoparticle aggregates were also maintained above 110 m^2/g, which enabled promising surface capabilities for future applications, in contrast to the commercial Degussa P25 TiO_2 nanoparticles of a typical surface area of approximately 60 m^2/g. Further increasing the water ratio slightly reduced the crystallite size, as evidenced by the small reducing of the main XRD peaks intensity. At the same time, the resulted spherical aggregates also experienced a small pore opening from 9.4 nm to 11.2 – 11.6 nm. The experimental phenomena suggest that the solvent mixture with a volume ratio of water : ethanol = 1:1 provides sufficient water molecules for the hydrolysis of all the titanium oligomers, as well as an adequate vapour pressure to facilitate the optimization of the development of a crystalline structure with mesoscopic porosity.

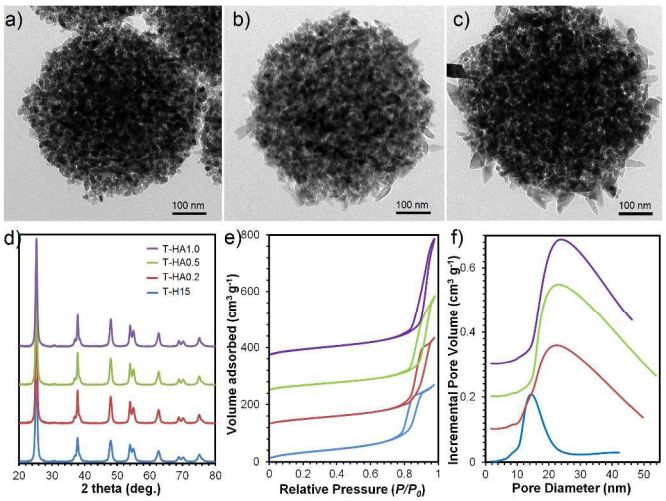

Fig 2. Mesoporous TiO_2 nanoparticle aggregates prepared with a varying amount of ammonia in solvothermal treatment in a 30 mL ethanol:water solvent (2:1 volume ratio): a) 0.2 mL; b) 0.5 mL; and c) 1.0 mL ammonia additives. Corresponding d) XRD patterns, e) nitrogen sorption isotherms and f) pore diameter distribution curves.

Table 2. Physical properties of the titanium oxide aggregates prepared with solvothermal treatment in presence of varying levels of ammonia.

Sample	Ammonia(mL)	S_{BET}(m^2/g)	PD(nm)	V_{sp} (cm^3/g)
T-H15	0	132.4	9.4	0.38
T-A0.2	0.2	113.3	14.1	0.48
T-A0.5	0.5	106.2	16.6	0.53
T-A1.0	1.0	128.0	17.4	0.65

Moreover, further addition of ammonia in the solvothermal process also enables fine tuning of pore size and particle shape of the final mesoporous structures, which was studied based on the ethanol : water = 1:1 solvent mixture. It was identified in Figure 2 that the use of additional ammonia of 0.2, 0.5 and 1 mL to the 30mL solution, changed the shape of the aggregated nanoparticles from spherical nanoparticles (**Sample T-H15**), to nanorods (**Sample T-A0.2 and Sample T-A0.5**), to nanospikes (**Sample T-A1.0**), respectively. This suggests that the additional ammonia accelerated the directional crystallization process and thus improved the specific crystal structural development. In Figure 2 d), growing diffraction intensity of the main XRD peaks, along with peak width narrowing, also confirms the well-established crystallinity under the influence of ammonia in the ethanol water solvent mixture. The small amount of ammonia changed the pH of the solvothermal solvent that promoted the hydrolysis of the titanium oligomers and the subsequent ripening of the growing crystals. Under the basic solvothermal environment, the preferential crystal growth is governed by the minimization of the total surface free energy, leading to the formation of rod-shaped titanium oxide nanoparticles with largely exposed low energy {101} facets, Figure S2. In a template-directed fabrication process, the template agent tends to form a barrier on the surface of titanium oligomers and block the access pathways for the solvent supply to the oligomer hydrolysis, which significantly supresses the subsequent crystalline growth. By contrast the template-free synthetic strategy in this work allows the solvent to reach the oligomers freely and enables simultaneous hydrolysis and crystal growth throughout the spherical aggregates, as noted in Figures 2 a) – c). This also facilitates a progressive pore opening while retaining the overall mesoporous structure – following the increasing ammonia concentration from 0 to 1.0 mL, the centre of pore diameter up-shifted from 10.9 to 17.4 nm, Figure 2 c). The type IV isotherms and H1 type hysteresis loops of nitrogen sorption confirm the mesoporous nature of the TiO_2 aggregates, Figure 2 e). The corresponding physical properties of **Samples T-A0.2, T-A0.5** and **T-A1.0** are listed in Table 2.

In addition, the ethanol and ammonia solvent mixture system (without water) was also studied in this work, which leads to the discovery of its great impact on the morphological evolution of the final hierarchical materials, as shown in Figure 3. Several interesting morphologies were achieved at different ammonia:ethanol volume ratios. A small amount of ammonia (1 mL) in the reaction solvent (of 30 mL) led to a spiky surface morphology of the aggregates, Figures 3 a) and b); it also dramatically improved the TiO_2 crystallinity (**Sample A-1**), compared to **Sample T-H0** and **Sample T-H1** synthesized from a pure ethanol solvent and an ethanol/water mixture with only 1 mL of water, as noted from the significantly enhanced XRD peak intensity, Figure 4 a). This can be attributed to the effect of water in the ammonia hydroxide solution (28% NH_3 in H_2O), which enabled the hydrolysis of the titanium oligomers and enhanced the crystal development. When the volume of ammonia was increased to 5 mL in the solvent mixture, tubular textures were formed over the surface of each sphere, as observed in Figure 3 c). High resolution TEM images in Figure 3 d) reveals that thin nanosheets curled up into tubular textures. Wormhole texture at the core area can also be identified from the high resolution TEM, which is responsible for the small mesopores. Associated with the formation of nanosheets, the appearance of a diffraction peak at $2\theta = 9.8^o$ in the low angle region and the reduced diffraction intensity of titanium oxide identity peaks indicate the co-existence of titanate and titania in the structure as the abundant ammonia prompted competitive reaction for ammonia titanate.

With the increase of the ammonia in the solvent mixture from 10 mL up to 20 mL, TEM and SEM observations in Figures 3 e)-h) and Figure S3 reveal a gradual change of morphology with more and more nanosheets generated on the surface of the spheres along with a gradually reduced core size. When the amount of ammonia increased to 20 mL, TEM and SEM images reveal that the entire sub-micron sized sphere was formed by flaky nanosheets network of an open porous structure. No morphology change can be found when ammonia

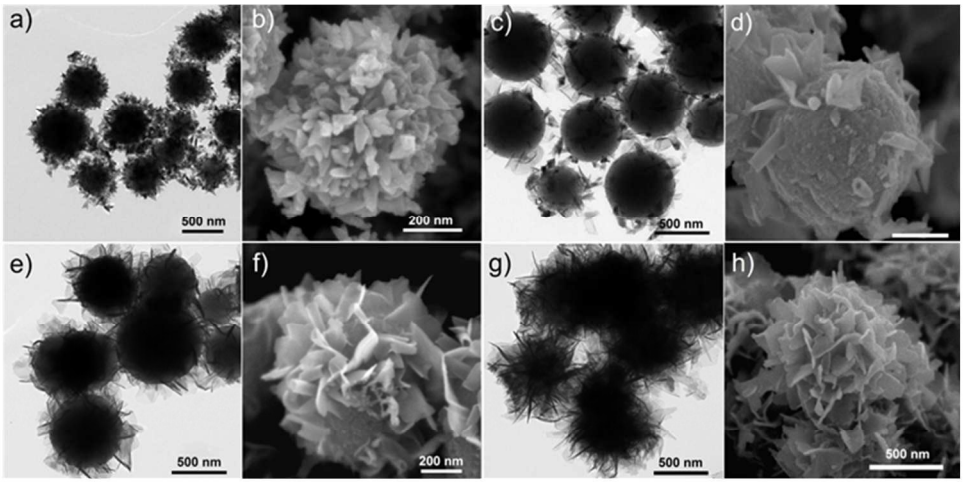

Fig 3. TEM and SEM images of structural evolution of the spherical TiO_2 as a function of ammonia content: a) and b) 1mL; c) and d) 5mL; e) and f) 10 mL; g) and h) 20 mL.

concentration was further increased (Figure S5). Aligned with the morphological change, the low-angle diffraction peak in XRD patterns becomes more intense and distinct with diminished TiO_2 diffraction peaks. The appearance of diffraction peaks at 2θ of 27.6°, 48.0° and 62.7° can be credited to layered ammonium titanate intercalated between octahedral TiO_6 layers and ammonium cations[16]. $TiO_{6-x}(OH)_x$ octahedral monomers generated from hydrolysis of the aggregated titanium oligomers quickly interacted with and were stabilized by the largely abundant NH_4^+ in the surrounding solution to form amorphous titanate via monomer condensation. The subsequent crystal growth and lattice re-orientation led to the extension of {100} facets and thus formation of ammonium titanate nanosheets, which explain the progressive morphology evolution with increasing ammonia concentration. Nitrogen sorption isotherms in Figure 4 b) reveal two hysteresis loops from all samples synthesized from the ethanol and ammonia solvent mixture, indicating the non-ordered mesoporous characteristics of the samples. A loop widening and up-shift to the higher P/P_o region along with increased ammonia concentration suggest an increase in pore diameter and pore volume. This was further confirmed by BET results, as listed in Table 3. The series of titanium hybrid structures exhibited superior surface areas ranging from 278.7 to 639.4 m^2/g with narrow mesopores of 3.7 to 7.7 nm. Further experimental studies were also carried out with equivalent concentration of NaOH instead of ammonia, as shown in Figure S5, which confirmed that the primary role of NH_4^+ in the structural evolution from spiky spheres to flaky texture with a nanosheets network (**Sample A-20**).

The as-synthesised titanium oxide based materials are of great interest for applications in environmental sustainability, which are also demonstrated as proof of concepts here. For instance, heavy-metal contamination (e.g. lead, cadmium, mercury and arsenic) in drinking water has quickly emerged as one of the main environmental issues that threats human health and is related to an increasing number of cases in cancer, neurological disorder and other diseases[17]. This has motivated the development focusing on more effective artificial adsorbent materials and water purification technologies[18]. **Sample T-H15** representing mesoporous titania oxide and **Sample A-20** representing open porous ammonium titanate were used to establish the feasibility of the hierarchical structures for heavy metal removal. Figure 5 a) shows the adsorption kinetics through time programmed lead (II) adsorption by commercial Degussa P25 TiO_2 nanoparticles, hierarchical mesoporous TiO_2 (**Sample T-H15**) and titanate (**Sample A-20**), respectively. The results show a rapid adsorption stage during the initial 10 mins, followed by adsorption equilibrium for P25 and a sharp drop of the adsorption rate for **Sample T-H15**. At the end of a two-hour test using a starting solution of 16.1 mg/L, the residual concentrations were of approximately 10.8, 7.7 and 0 mg/L for P25, T-H15 and A-20, respectively.

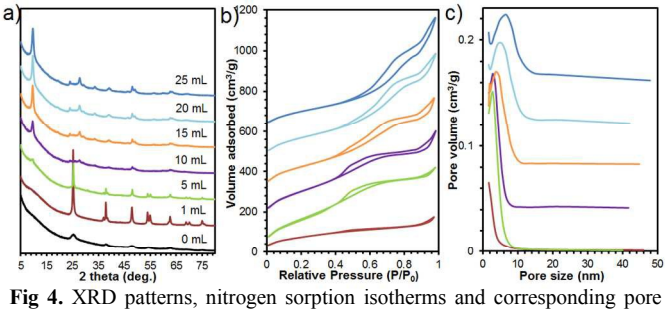

Fig 4. XRD patterns, nitrogen sorption isotherms and corresponding pore size distribution of spheres with flaky structures prepared with a varying amount of ammonia in solvothermal treatment.

Table 3. Physical properties of the spherical titanium oxide aggregates prepared with solvothermal treatment in the presence of a varying amount of ammonia.

Sample	Ammonia (mL)	S_{BET} (m^2/g)	PD (nm)	V_{sp} (cm^3/g)
A-1	1.0	278.7	4.4	0.22
A-5	5.0	639.4	3.7	0.58
A-10	10.0	586.2	4.4	0.63
A-15	15.0	477.4	5.3	0.67
A-20	20.0	451.3	6.3	0.79
A25	25.0	360.6	7.7	0.84

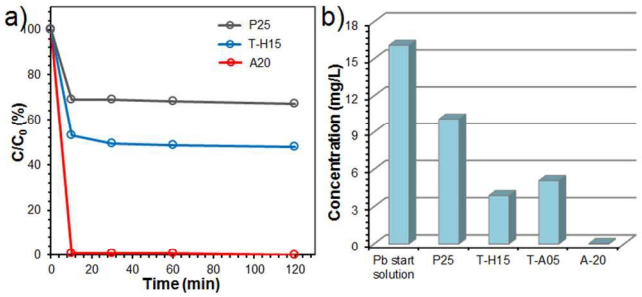

Fig 5. a) Kinetics of adsorption of heavy metal (Pb^{2+}) and b) overnight (16 hours) adsorption, by titanium oxide and titanate materials at room temperature.

In Figure 5 b), the residual concentrations from an overnight adsorption test using the same starting concentration of lead nitrate reveals that adsorption equilibriums of P25, the **Sample T-H15** and **Sample T-A0.5** are at 10.1, 3.9 and 5.1 mg/L, respectively. The result suggests that the superior specific surface areas of **Sample T-H15** (132.4 m^2/g) and **Sample T-A0.5** (106.2 m^2/g) in comparison with P25 (61.3 m^2/g) are primarily responsible for the greatly improved adsorption

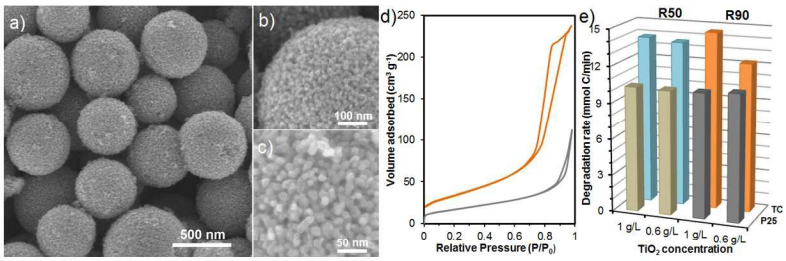

Fig 6. a) – c) SEM images of calcined mesoporous TiO_2 nanoparticle aggregates, **Sample TC**. d) Nitrogen sorption isotherms and e) Formic acid photocatalytic degradation rates at R50 and R90 (60 µL, 20000 ppm carbon) using calcined **Sample TC** and P25 nanoparticle with varying concentrations.

abilities. **Sample T-H15** with the mesoporous structure took much longer to reach adsorption equilibrium; as a result, more diffusion time is needed for lead ions to penetrate through the mesoscopic tunnels formed among the interfaces of the nanoparticles, which fill up the interior of the aggregates. In contrast, as the layered titanate offers a relatively open structure and greater surface area than the nanoparticle aggregates, **Sample A-20** exhibited the most efficient and effective adsorption ability in comparison with **Sample T-H15** and P25. Generally, nanoscale artificial adsorbents, such as P25, can easily escape from the filter bed causing flow pressure drop in a flow-through adsorption system and are also difficult to be separated from a suspension system for water purification. By contrast, the unique combination of the sub-micron sized building block with superior nanoscale porosity provides the as-synthesized hierarchical materials with great advantages for applications in both flow-through and suspension water purification systems.

Different from inorganic pollutants, organic pollutants can be removed from water through photo-oxidation on the surface of a photocatalyst, e.g. TiO_2, utilizing natural or artificial light sources such as the abundant sunlight or a UV lamp[18]. Among the as-synthesised hierarchical structures, the mesoporous TiO_2 aggregates synthesised from the ethanol and water system possess desirable thermal stability for practical photocatalytic applications, which generally involves a thermal regeneration process of the photocatalytic materials. Before the photocatalytic reaction, **Sample T-H15** was thermally treated at 500 ^oC for 30 min to remove potentially trapped organic impurities and solvents from the material surface. In Figure 6 a), an SEM image displays the overall morphology of the **Sample TC** after the calcination, showing unchanged sub-micron spherical shape and aggregation feature. In comparison

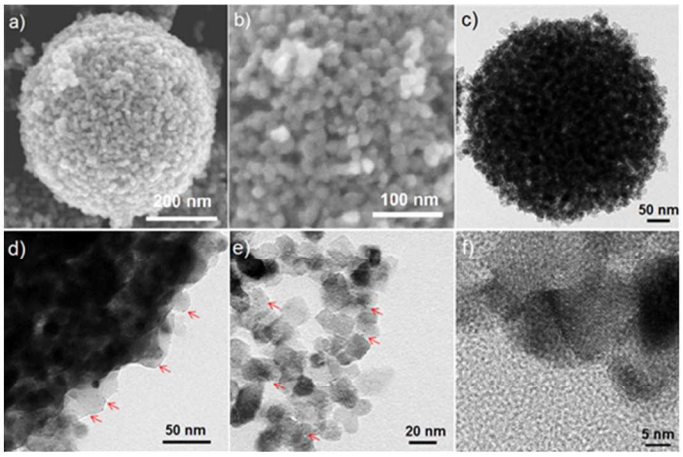

Fig 7. SEM and TEM images of mesoporous TiO_2 nanoparticle aggregates (Sample T-H15) with deposited Pt nano-clusters.

to the parent **Sample T-H15**, the strengthened inter-particle contrasts and much clear particle features in the **Sample TC,** Figures 6 b) and c), resulted from further-developed nanoparticle crystallinity and crystalline refinement during the calcination. **Sample TC** also shows a typical type IV isotherm with a H1 hysteresis loop of nitrogen sorption, which reflects the unaffected mesoporous nature. After calcination, the specific surface area slightly dropped to 100.6 m^2/g, which is still far beyond that of 61.3 m^2/g from P25. Large surface area benefits photocatalytic reactions, as more reaction species are able to anchor at the active sites on the surface of TiO_2. In the subsequent photooxidation of formic acid by **Sample TC** and P25, despite that the rutile/anatase interphase in P25 generally acts as a synergic electron-hole pair separation driving force, the mesoporous **Sample TC** still shows a higher formic acid degradation rate than P25, Figure 6 e), where the photooxidation rates are shown at half reaction (R50) and 90% reaction (R90) for two different solid loadings of 1 and 0.6 g/L, respectively.

In addition, the thermally stable mesoporous structure and superior specific surface area are also promising for the generation of highly dispersed co-catalyst/-photocatalyst on the surface. Figure 7 shows SEM and TEM images of **Sample T-H15** with 1at% Pt deposition, where there are no evident changes of morphological or surface features. Most Pt nanoparticles are of size down to only a few nanometers and finely dispersed on the surface of the TiO_2 nanoparticles giving slightly darker contrast in the TEM images, than the semiconductor TiO_2. Figure 7 f) shows three slightly larger Pt with droplet size of approximately 5 - 10 nm capped on TiO_2 nanoparticles. Hydrogen temperature programmed reduction of 1 and 5 at% deposition of Pt on both **Sample T-H15** and P25 were shown in Figures 8 a) and b), respectively. As smaller platinum species nanoparticles has a higher proportion of surface atoms for stronger capping with oxygen of TiO_2 at the particle interfaces, it will be more difficult to reduce the platinum species or reduce them at a higher temperature, in comparison with the larger platinum species[20]. In the H_2-TPR results, mesoporous TiO_2 (**Sample T-H15**) with 1 at% Pt shows two main peaks at approximately 320 and 610 ^oC, respectively, while P25 gives main peaks at approximately110 ^oC and 525 ^oC. This indicates that the Pt nanoparticles are better dispersed in **Sample T-H15** than in P25. The same phenomena were also observed in 5 at% Pt deposited **Sample T-H15** and P25, which confirm the mesoporous TiO_2 as a promising candidate for catalytic/photocatalytic reactions with superior surface capabilities.

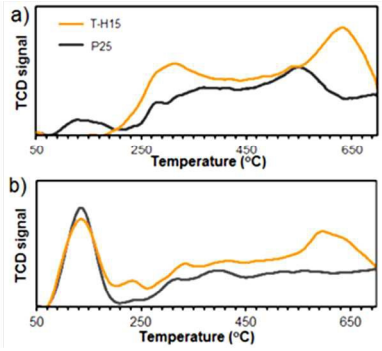

Fig 8. Hydrogen temperature programed reduction of a) 1% and b) 5% Pt-deposited mesoporous TiO_2 nanoparticle aggregates (Sample T-H15) and P25 TiO_2 nanoparticles.

Conclusions

Morphology and crystallinity are important for functional nanostructures, such as TiO_2. It has been clearly shown that tuning the solvent mixture in solvothermal reaction has enabled a sophisticated control of the hierarchical morphology of the titanium oxide hybrids products by the facile and effective template-free synthesis strategy. This is facilitated by changes of the solvent vapour pressure and the amount of water in the reaction system, which governs the hydrolysis of titanium oligomers and subsequent growth of the crystalline phase. Such structures show exceptionally high specific surface area and well-developed crystal interfaces, leading to large enhancement of heavy metal removal, organic matter degradation and catalyst dispersion. The synthesis route and the resulting titanium oxide hybrid structures demonstrate their promising potentials for environmental sustainability. Future experimental studies will focus on the morphological evolution following the change of reaction temperature or time, which is of great interest for further scientific insight into the transformation mechanism of the crystalline structure, and improved understanding of the material properties that would greatly contribute to full industrial exploration of such structures.

Acknowledgements

The authors acknowledges the support for the "4G-Photocat" project from the European Commission's Seventh Framework Programme (FP7) for Research and Technological Development (Grant No.: 309636).

Notes and references

[a] School of Chemical Engineering, University of New South Wales, Kensington, Sydney 2052, Australia.
[b] Department of Chemistry, University College London, 20 Gordon Street, London, WC1H 0AJ, UK.
[c] International Joint Research Laboratory for Quantum Functional Materials of Henan, and School of Physics and Engineering, Zhengzhou University, Zhengzhou, 450001, China.
† Equal first authors.
‡ Electronic Supplementary Information (ESI) available: Experimental details. See DOI: 10.1039/b000000x/

1 a) R. Lakes, *Nature*, 1993, **361**, 511; b) W. A. Lopes, H. M. Jaeger, *Nature*, 2001, **414**, 735; b) J. Jiang, J. L. Jorda, J. Yu, L. A. Baumes, E. Mugnaioli, M. J. Diaz-Cabanas, U. Kolb, A. Corma, *Science*, 2011, **333**, 1131; c) A. H. Gröschel, A. Walther, T. I. Löbling, F. H. Schacher, H. Schmalz, A. H. E. Müller, *Nature*, 2013, **503**, 247; d) W. L. Noorduin, A. Grinthal, L. Mahadevan, J. Aizenberg, *Science*, 2013, **340**, 832.

2 a) H. G. Yang, C. H. Sun, S. Z. Qiao, J. Zou, G. Liu, S. C. Smith, H. M. Cheng, G. Q. Lu, *Nature*, 2008, **453**, 638; b) X. Zhang, D. Liu, D. Xu, S. Asahina, K. A. Cychosz, K. V. Agrawal, Y. A. Wahedi, A. Bhan, S. A. Hashimi, O. Terasaki, M. Thommes, M. Tsapatsis, *Science*, 2012, **336**, 1684; c) J. B. Joo, M. Dahl, N. Li, F. Zaera, Y. Yin, *Energy Environ. Sci.*, 2013, **6,** 2082.

3 a) D. Chen, L. Cao, T. L. Hanley, R. A. Caruso, *Adv. Funct. Mater.* 2012, **22**, 1966; b) A. M. Youssef, F. M. Malhat, *Macromol. Symp.* 2014, **337**, 96.

4 a) W.-Q. Wu, H.-L. Feng, H.-S. Rao, Y.-F. Xu, D.-B. Kuang, C.-Y. Su, *Nat. Commun.*, 2014, 5:3968; c) A. M. Cant, F. Huang, X. L. Zhang, Y. Chen, Y.-B. Cheng, R. Amal, *Nanoscale*, 2014, **6**, 3875.

5 a) J. N. Schrauben, R. Hayoun, C. N. Valdez, M. Braten, L. Fridley, J. M. Mayer, *Science*, 2012, **336**, 1298; b) Y. Zhao, Q. Chen, F. Pan, H. Li, G. Q. Xu, W. Chen, *Chem. Eur. J.* **2015**, DOI: 10.1002/chem.201400120; c) H. Tian, X. L. Zhang, J. Scott, C. Ng, R. Amal, *J. Mater. Chem. A.*, 2014, **2**, 6432.

6 a) S. U. M. Khan, M. Al-Shahry, W. B. I. Jr. *Science*, 2002, **297**, 2243; b) J. H. Pan, X. Z. Wang, Q. Huang, C. Shen, Z. Y. Koh, Q. Wang, A. Engel, D. Bahnemann, *Adv. Funct. Mater.* 2014, **24**, 95; c) X. L. Zhang, F. Huang, Y. Chen, Y.-B. Cheng, R. Amal, *RSC Adv.*, 2013, **3**, 17003.

7 a) Y.-M. Jiang, K.-X. Wang, H.-J. Zhang, J.-F. Wang, J.-S. Chen, *Sci. Rep.*, 2014, 3:3490; b) H. Liu, Z. Bi, X.-G. Sun, R. R. Unocic, M. P. Pranthaman, S. Dai, G. M. Brown, *Adv. Mater.* 2011, **23**, 3450; c) G. Kim, C. Jo, W. Kim, J. Chun, S. Yoon, J. Lee, W. Choi, *Energy Environ. Sci.*, 2013, **6**, 2932.

8 a) H. Kim, M.-Y. Cho, M.-H. Kim, K.-Y. Park, H. Gwon, Y. Lee, K. C. Roh, K. Kang, *Adv. Energy Mater.* 2013, **3**, 1500; b) X. Lu, G. Wang, T. Zhai, M. Yu, J. Gan, Y. Tong, Y. Li, *Nano Lett.* 2012, **12**, 1690.

9 a) S.-J. Bao, C. M. Li, J.-F. Zang, X.-Q. Cui, Y. Qiao, J. Guo, *Adv. Funct. Mater.* 2008, **18**, 591; b) J. Chen, Z. Hua, Y. Yan, A. A. Zakhidov, R. H. Baughman, L. Xu, *Chem. Commun.* 2010, **46,** 1872; c) G. T. S. How, A. Pandikumar, H. N. Ming, L. H. Ngee, *Sci. Rep.*, 2014, 4:5044.

10 J. Peng, L.-N. Feng, Z.-J. Ren, L.-P. Jiang, J.-J. Zhu, *Adsorption*, 2008, **14**, 21.

11 a) J. Sun, J. Zhang, M. Zhang, M. Antonietti, X. Fu, X. Wang, *Nat. Commun.*, 2012, 3:1339; b) X. L. Zhang, Z. Zhang, F. Huang, P. Bauerle, U. Bach, Y.-B. Cheng, *J. Mater. Chem.,* 2012, **22**, 7005; c) Y. Chen, F. Huang, D. Chen, X. L. Zhang, Y.-B. Cheng, R. A. Caruso, *Chemsuschem.* 2012, **22**, 1966.

12 a) X. L. Zhang, R. Qiao, J. C. Kim, Y. S. Kang, *Cryst. Growth Des.* 2008, **8**, 2609; b) X. L. Zhang, R. Qiao, R. Qiu, Y. Li, Y. S. Kang, *J. Phys. Chem. A* 2007, **20**, 4195.

13 X. L. Zhang, Y. Chen, A. Cant, F. Huang, Y.-B. Cheng, R. Amal, *Part. Part. Syst. Charact.*, 2013, **30**, 754.

14 a) X. Jiang, T. Herricks, Y. Xia, *Adv. Mater.* 2003, **15,** 1205; b) Y. Wan, D. Zhao, *Chem. Rev.* 2007, **107**, 2821; c) D. Chen, L. Cao, F. Huang, P. Imperia, Y.-B. Cheng, R. A. Caruso, *J. Am. Chem. Soc.,* 2010, **132**, 4438.

15 a) Wu, C.; Xie, Y.; Lei, L.; Hu, S.; OuYang, C. *Adv. Mater.* 2006, **18**, 1727; b) X. L. Zhang, R. Qiao, J. C. Kim, Y. S. Kang, *Cryst. Growth Des.,* 2008, **8**, 2609; c) Yu, J.; Guo, H.; Davis, S. A.; Mann, S. *Adv. Funct. Mater.* 2006, **16**, 2035.

16 a) B. Zhao, F. Chen, Y. C. Jiao, J. L. Zhang, *J. Mater. Chem.* 2010, **20**, 7990; b) L. Cao, D. Chen, R. A. Caruso, *Angew. Chem. Int. Ed.* 2013, **52**, 10986.

17 a) L. Järup, *Brit. Med. Bull.* 2003, **68**, 167; b) S. Cheng, W. Grosse, F. Karrenbrock, M. Thoennessen, *Ecological Eng.*, 2002, **18**, 317.

18 a)Y. X. Zhang, Y. Jia, Z. Jin, X. Y. Yu, W. H. Xu, T. Luo, B. J. Zhu, J. H. Liu and X. J. Huang. *CrystEngComm*, 2012, **14**, 3005; b) Y. X. Zhang, Z. L. Liu, B. Sun, W. H. Xu and J. H. Liu. *RSC.Adv.,* 2013, **3**, 23197; c) Y. X. Zhang, X. Y. Yu, Z. Jin, Y. Jia, W. H. Xu, T.

Luo, B. J. Zhu, J. H. Liu and X. J. Huang. *J. Mater. Chem.*, 2011, **21**, 16550.

19 a) L. W. Miller, M. I. Tejedor-Tejedor, M. A. Anderson, *Environ. Sci. Technol.* 1999, **33**, 2070.

20 a) C. Zhang, H. He, K.-i. Tanaka, *Appl. Catal. B-Environ.*, 2006, **65**, 37; b) C.-H. Lin, J.-H., Chao, C.-H. Liu, J.-C., Chang, F.-C., Wang, *Langmuir*, 2008, **24**, 9907.